Flow Turbulence Combust
DOI 10.1007/s10494-012-9395-y

The Oriented-Eddy Collision Turbulence Model

Michael B. Martell · J. Blair Perot

Received: 28 September 2011 / Accepted: 11 April 2012

Abstract The Oriented-Eddy Collision (OEC) model treats turbulent flow as a non-Newtonian fluid where the average behavior of turbulence is modeled as a collection of interacting fluid particles which have inherent orientation. The model is derived from the two-point velocity correlation transport equation, and has the form of a collection of Reynolds-stress transport equations, with one set of transport equations for each representative eddy direction. The addition of eddy orientation information adds important physics to the model and allows the model to represent structural (two-point) information about the turbulence. This structural information is sufficient to allow the model to capture the effect of external forces and imposed mean strains (such as rapid distortion theory) exactly. The only physical effects that must be empirically modeled are those that are due to turbulence-turbulence interactions, referred to as eddy collisions. The performance of the model in a number of canonical flow situations is presented.

Keywords Turbulence · Turbulence modeling · PDF collision · Eddies · Two-point correlations

1 Introduction

One fairly limiting aspect of most turbulence models is that they do not capture the linearized Navier-Stokes equations. In theory, a linear equation system should not require a model at all (and should therefore be trivial to model) as all modes or solutions to the linear equations are uncoupled and do not interact with one another.

M. B. Martell · J. B. Perot (✉)
The University of Massachusetts Amherst,
168 Governor's Drive, Amherst, MA 01003, USA
e-mail: perot@ecs.umass.edu

Published online: 04 May 2012

If one considers the case of incompressible fluid flow, the transport equation for the fluctuating velocity (or turbulence) in a noninertial reference frame is

$$\frac{\partial u_i'}{\partial t} + \overline{u}_j u_{i,j}' = -\overline{u}_{i,j} u_j' + 2\varepsilon_{ijl}\Omega_l u_j' + \nu u_{i,jj}' - p_{,i}' - \left(u_i' u_j' - \overline{u_i' u_j'}\right)_{,j} \tag{1}$$

where $\overline{u}_j$ is the mean velocity, u_j' the fluctuating velocity, v the kinematic viscosity, ε_{ijl} the permutation tensor and Ω_l is the external system rotation rate. This equation also assumes constant viscosity and density, so the fluctuating incompressibility constraint also holds, $u_{i,i}' = 0$, and determines the fluctuating pressure, p'. Note that only the final term is nonlinear. If any of the other terms on the right hand side are very large, then the last term can be neglected, the equation system becomes linear, and it is sometimes even analytically solvable. The classic case of exact turbulence solutions is rapid distortion theory (RDT), where the first term on the right hand side (involving the mean strain) is large.

It is important to note that the pressure term is always the same order of magnitude as the largest term on the right hand side of Eq. 1, and therefore never can be neglected. It is key to obtaining the correct solution. The pressure is also the key difficulty with existing turbulence models. Reynolds stress transport (RST) models are derived directly from Eq. 1. They capture the first term on the right-hand-side (the production term) exactly, but they model the pressure term (which is the same size and therefore always important). Reynolds stress transport models therefore cannot represent the simple case of linearized turbulence (RDT) properly. In fact, it has been shown that models for the pressure effects that only involve the fluctuating velocity are fundamentally incapable of representing all RDT flows correctly [1] regardless of how many tuning constants are involved.

Fundamentally, the problem stems from the nature of the fluctuating pressure which is elliptic and depends strongly on the neighboring velocity field, not the local one. The pressure therefore depends on the shape or structure of the turbulent eddies present in a given flow. The eddies generated by thermal buoyancy in the atmosphere tend to be oblate (flattened) spheroids, while the eddies generated by strong shear tend to be prolate (elongated) spheroids. The local velocity fluctuation levels (Reynolds stresses) may be identical in both flows; however, the turbulence (and therefore the mean flow) evolves differently in the two cases. A model which can predict RDT exactly must somehow capture the effect of these different turbulent eddy structures correctly.

The focus of turbulence modeling has long been on the Reynolds stress tensor (or its divergence, the body force vector [2]) as this is the critical variable needed to predict the mean flow evolution. What has recently become clear is that predicting the Reynolds stress tensor evolution requires knowledge of the local turbulent structure. The equations cannot be closed at the Reynolds stress tensor level such that they predict linear effects (RDT) without including structural information. Adding more information leads to a closure approach which captures a great deal more of the physics exactly (including the RDT limit). In this work, it is hypothesized that the remaining physics not represented directly by the Reynolds stress tensor and additional structural information is relatively easy to model accurately.

1.1 Models for linear turbulence

The first attempt to model RDT exactly was by Reynolds and Kassinos (see [3] and the many references therein). Reynolds and Kassinos noted that the stress tensor (velocity fluctuations) did not contain enough information to capture linearized turbulence exactly. They suggested a model which transports a single, rank two tensor, the "eddy axis tensor", characterizing the shape and orientation of a turbulent eddy. Their model employs algebraic equations of state to obtain the Reynolds stress tensor and uses two scalar transport equations containing information about the dimensionality and componentality of the turbulence. The model managed to capture many linear turbulence cases exactly, which was the first ever demonstration of an RST-like turbulence model providing accurate solutions in this limit of turbulence. Their work produced a powerful idea: perhaps the limitations of previous turbulence models lie not in the model but instead was instead due to the absence of turbulence structure.

Reynolds and Kassinos furthered this idea with the Particle Representation Model (PRM) [4]. Kassinos and Akylas later extended it with the Interacting Particle Representation Model (IPRM) [5]. The main difference between the PRM / IPRM approaches and the Oriented-Eddy Collision model lies in the way the models average over turbulent structure. The OEC approach averages over structures which have the same orientation while PRM/IPRM approaches do not. Such averaging is discussed in several of PRM papers, but is not used in practice. In addition, the OEC approach folds both structure magnitude and direction into one quantity, the eddy orientation vector. The PRM approach tends to use unit vectors.

Pope and Van Slooten [6] extended these ideas to the probability density function (pdf) modeling framework. A typical pdf model computes the probability of a certain velocity fluctuation at a certain location and time. In [3] the pdf was expanded to compute the probability of a certain velocity *and* a certain "wavevector" at some location and time (a 10 dimensional space). This model is also capable of exactly predicting linearized turbulence (or rapid distortion theory) in homogeneous turbulence.

The OEC model incorporates turbulence structure information into the model. In this case, the model is derived from the exact two-point velocity correlation transport equation. Two-point correlations are an intuitive representation for turbulence structure. If two separated points have velocities that are closely correlated, those two points have a high probability of being in the same eddy. When a correlation gets close to zero that represents the final extent of the average eddy. It is therefore possible that two-point correlations are a reasonable environment in which to construct a general model for engineering applications (with inhomogeneous turbulence, walls, and other complications), that is still capable of capturing rapid distortions (the linearized limit) exactly.

The derivation of the model is presented in Section 2. The final result of this section is a collection of Reynolds stress transport (RST) equations. There is one tensor transport equation for each representative eddy orientation. Many existing computational fluid dynamics (CFD) codes have RST models implemented already. This structure of the OEC model makes it reasonably simple to incorporate into existing CFD infrastructure. To illustrate this, the results in Section 3 were computed

with the OEC model implemented in the open source collection of computational fluid dynamics libraries, OpenFoam [7, 8]. Section 3 details canonical test cases employed to benchmark the OEC model. Exact results in the RDT limit are shown as well as other important limits, such as rotating decay and return to isotropy, that test the other (inexact) aspects of the model. A short discussion of the results is presented in Section 4.

2 The Oriented-Eddy Collision Model

The general form for the exact but unclosed equation for the evolution of the two-point velocity correlation tensor is

$$\begin{aligned}\frac{\partial}{\partial t}Q_{ij}(x,r)+\bar{u}_k(x)\frac{\partial Q_{ij}}{\partial x_k} &= -\left(\bar{u}_{i,k}(x)+2\varepsilon_{kil}\Omega_l\right)Q_{kj}-\left(\bar{u}_{j,k}(\widetilde{x})+2\varepsilon_{kjl}\Omega_l\right)Q_{ik}\\ &\quad+\left(\bar{u}_k(x)-\bar{u}_k(\widetilde{x})\right)\frac{\partial Q_{ij}}{\partial r_k}-\left(\frac{\partial Q_{(ik)j}}{\partial x_k}-\frac{\partial Q_{(ik)j}}{\partial r_k}\right)\\ &\quad-\frac{\partial Q_{i(kj)}}{\partial r_k}-\left(\frac{\partial\overline{pu'_j}}{\partial x_i}-\frac{\partial\overline{pu'_j}}{\partial r_i}\right)-\frac{\partial\overline{u'_ip}}{\partial r_j}\\ &\quad+\nu\left(\frac{\partial^2 Q_{ij}}{\partial x_k\partial x_k}-2\frac{\partial^2 Q_{ij}}{\partial x_k\partial r_k}+2\frac{\partial^2 Q_{ij}}{\partial r_k\partial r_k}\right)\end{aligned}\tag{2}$$

In the context of two point correlations, x is the vector representing the physical location of the first point in a two point correlation and r a vector pointing toward the second point $\widetilde{x}\equiv x+r$. Note that explicit dependence on x and $\widetilde{x}$ is implied by the index order and is not explicitly stated. In Eq. 2 above, the notation $Q_{(ik)j}$ implies a triple correlation viz. $\overline{u'_i(x)u'_k(x)u'_j(\widetilde{x})}$, and similarly $Q_{i(kj)}=\overline{u'_i(x)u'_k(\widetilde{x})u'_j(\widetilde{x})}$. Note that an external forcing given by the term $\overline{f_i(x)u'_j(\widetilde{x})}+\overline{u'_i(x)f_j(\widetilde{x})}$ has not been explicitly included. In the homogeneous turbulence limit, where the spatial derivatives of turbulence quantities are zero and the mean flow gradients are constant, this becomes [9],

$$\begin{aligned}\frac{\partial}{\partial t}Q_{ij}(x,r) &= -\left(\bar{u}_{i,k}+2\varepsilon_{kil}\Omega_l\right)Q_{kj}-\left(\bar{u}_{j,k}+2\varepsilon_{kjl}\Omega_l\right)Q_{ik}-r_l\frac{\partial\bar{u}_k}{\partial x_l}\frac{\partial Q_{ij}}{\partial r_k}\\ &\quad+\left(\frac{\partial\overline{u'_jp}(\widetilde{x},-r)}{\partial r_i}-\frac{\partial\overline{u'_ip}}{\partial r_j}\right)\\ &\quad+2\nu\frac{\partial^2 Q_{ij}}{\partial r_k\partial r_k}+\left(\frac{\partial Q_{(ik)j}}{\partial r_k}-\frac{\partial Q_{i(kj)}}{\partial r_k}\right)\end{aligned}\tag{3}$$

For an incompressible flow it can be shown that

$$\frac{\partial Q_{ij}}{\partial r_j}=0\tag{4}$$

which allows the pressure-velocity correlations (4th term on the right hand side of Eq. 3) to be determined. In fact, the only unclosed terms in the two-point evolution

equation are the terms involving the two-point triple-velocity correlations (the last term in Eq. 3). If the triple-velocity correlations are neglected, Eq. 3 represents linearized turbulence (RDT).

2.1 Linear OEC model

To derive the model we use the assumption that the correlations can be decomposed using

$$Q_{ij} = \frac{1}{N}\sum_{n=0}^{N} R_{ij}^{n}(t)\frac{\partial F}{\partial \eta}\left(\eta^{n}\right) \text{ and } \overline{u_i' p} = \frac{1}{N}\sum_{n=0}^{N} w_i^{n}(t) F\left(\eta^{n}\right) \tag{5}$$

where $\eta^n = \left|\mathbf{r}\cdot\mathbf{q}^n\right|$ and $\mathbf{q}^n(t)$ is the eddy orientation direction. The shape function, $F = F(\eta)$ is some function (like a decaying exponential $\frac{\partial F}{\partial \eta} = e^{-\eta}$) that has a derivative equal to unity at $\eta = 0$ and which drops quickly off to zero at infinity. It is unitless, as is η^n. The orientation vector $\mathbf{q}^n$ has units of inverse length. The function F implies an assumption as to the shape of the two-point correlation subsets. No assumptions are made about the variance. In each direction, given by the orientation vector $\mathbf{q}^n$, that eddy's contribution to the correlation will drop off according to the inverse of the length of $\mathbf{q}^n$ in the direction of $\mathbf{q}^n$ and will not approach zero in the plane perpendicular to $\mathbf{q}^n$. The summation allows us to have different correlation lengths in different directions. As long as the number of eddies, N, is very large, the total correlation will still go towards zero at infinite separation even though individual contributions to the summation may not. In practical computations, a finite sum (often around 20–100 eddies) is used, and the modeled correlations drop to a maximum of 5%–1% at infinite separation. In what follows the orientation superscript, n, is dropped, and summation is assumed to imply over all orientations. Subscripts continue to refer to Cartesian tensor notation. For the cases considered in this work, the same N eddies occupy all locations in space. This decomposition does not require homogeneity. For the homogeneous flows considered here, all eddy orientation vectors $\mathbf{q}^n$ are initially distributed in a uniform manner on a unit sphere (see Section 2.3).

The decomposition given by Eq. 5 is powerful. First, it allows complex correlations to be represented simply. When Eq. 5 is plugged into the two-point evolution equations for homogeneous turbulence (Eqs. 3 and 4) the equations for RDT are recovered (see Appendix A for the derivation). For RDT these equations do not depend at all on the choice of F. If the two-point correlation is required, a form for F must be assumed. If the Reynolds stress tensor is the only necessary quantity (which is often the case) then $\overline{R}_{ij} = Q_{ij}(\mathbf{r} = 0) = \frac{1}{N}\sum R_{ij}$ and the system is again independent of the choice of F.

Appendix A shows that the following equations for the decomposition coefficients is a solution for the inviscid two-point RDT equations (Eqs. 3 and 4),

$$\frac{DR_{ij}}{Dt} = \left[\overline{u}_{i,k} + \left(\frac{q_i q_l}{q^2} - \delta_{il}\right) 2\overline{u}_{l,k}^{*}\right] R_{kj} + \left[\overline{u}_{j,k} + \left(\frac{q_j q_l}{q^2} - \delta_{jl}\right) 2\overline{u}_{l.k}^{*}\right] R_{ki} \tag{6a}$$

$$\frac{Dq_i}{Dt} = -q_k \overline{u}_{k,i} \tag{6b}$$

where δ_{ij} is the Kronecker delta, $\overline{u}_i$ the mean velocity, and $\overline{u}^*_{i,j} = \overline{u}_{i,j} + \varepsilon_{ikj}\Omega_k$ the transformation-invariant velocity gradient tensor accounting for system rotation effects. Equation 6a accounts for the advection and production of the Reynolds stress tensor as well as the rapid pressure-strain redistribution. Equation 6b is the same as the equation for the normal vector of passive disk embedded in a mean flow. As a result we frequently refer to our eddies as disk-like (or planar) in shape. This does *not* imply that the two-point correlation is disk-like, as it is a sum over many eddies all located at the same place and time.

This system (Eqs. 6a and 6b) can be solved numerically to obtain exact RDT results. The form of the equations is identical in form to the analytical Fourier solution for exact rapid distortion theory from Pope [10]. However, it should be remembered that Eqs. 6a and 6b were not derived with any relation to Fourier space, and the ideas behind their construction can therefore be relatively easily extended to Eq. 2 and general turbulence situations. While not common, other solutions in the form of correlations exist, such as those proposed by Deissler [11].

2.2 The complete OEC model

For a full OEC model, the equation system must be generalized to account for diffusion, as well as the nonlinear affects of turbulent dissipation, and return to isotropy. These effects may appear in either or both Eqs. 6a and 6b. The turbulent dissipation term is discussed in detail in de Bruyn Kops and Perot [12]. In summary, the decay equations are

$$\frac{\partial R_{ij}}{\partial t} = -\left(2\alpha\nu\overline{q^2} + \frac{1}{\tau_R}\right) R_{ij} \tag{7a}$$

$$\frac{\partial q_i}{\partial t} = -\frac{1}{3}\left(2\alpha\nu\overline{q^2} + \frac{1}{\tau_R}\right) q_i \tag{7b}$$

where $1/\tau_R$ is the inverse turbulent timescale. These equations will produce the exact decay behavior for isotropic turbulence in both the high Reynolds number (Re) limit and the low Reynolds number limit. The constant α, which is currently set to 15.0, determines the Reynolds number at which the switch from high to low Reynolds number behavior occurs. The fraction 1/3 is exact for Saffman decay [13, 14] (a low wavenumber spectrum of k^2) which was determined to be appropriate for turbulence generated by walls [15]. Note that a fraction of 1/5 is correct for Kolmogorov/Bachelor decay (a low wavenumber spectrum of k^4), if that is desired. It is important to note that the viscous inverse time-scale is $2\alpha\nu\overline{q^2}$, and the turbulent inverse time-scale is $1/\tau_R$, and their effect is additive in this model.

The positive definite inverse eddy turnover time is modeled as $1/\tau_R = \left(\overline{K}\overline{q^2}\right)^{1/2} = \overline{K}^{1/2}\left(\frac{1}{N}\sum q^2\right)^{1/2}$. The average kinetic energy over all eddies is defined as $\overline{K} = \frac{1}{N}\sum\left(\frac{1}{2}R_{ii}\right)$ where N is the number of eddies employed in a given simulation of turbulent flow. Note that the overbar is used to indicate a quantity which has been averaged over all eddies. The quantities of interest to the engineer are not the individual eddies' statistics but those quantities averaged over all eddies. For example, $\overline{R}_{ij} = \frac{1}{N}\sum R_{ij}$ is the familiar Reynolds stress tensor.

Return-to-isotropy is another important result of the nonlinear turbulence-turbulence interactions. A number of return-to-isotropy models are considered in

Chartrand and Perot [16], including one just on the cusp of strong realizability that has no tunable constants. In this work a modified version of Rotta's linear return-to-isotropy model [17] is employed for the orientation stresses in Eq. 6a.

$$-\frac{1}{\tau_R}\left(\frac{C_R}{1+C_B\nu/\nu_T}\right)\left[R_{ij}-\overline{K}\left(\delta_{ij}-\frac{q_iq_j}{q^2}\right)\right] \tag{8}$$

In expression (8), C_R and C_B are tunable constants. The first is quite important and is set to 1.375. The latter, set to 1.0, is only active in the very low Reynolds number limit where it sets the Re where return-to-isotropy goes to zero, recalling that at very low Reynolds numbers the flow approaches Stokes flow and is once again linear with effectively no modal interactions.

The positive definite turbulent viscosity is given by $\nu_T = \left(\overline{K^2}/\overline{Kq^2}\right)^{1/2}$. Note that Reynolds stress isotropy is typically defined as the scalar kinetic energy multiplied by the identity tensor, $\frac{2}{3}\overline{K}\delta_{ij}$. In expression (8), however, this tensor is modified by the normalized outer product of the orientation vector q_iq_j/q^2. This modification of the term means that this return term is always orthogonal to the orientation vector. Appendix A shows how orthogonality of the orientation stress and the orientation vector is a direct result of the fluctuating incompressibility constraint. This form of the return term means that this orthogonality is maintained even during return-to-isotropy. While the two terms are similar in form, note that the formulation of the eddy viscosity is not related to the formulation of the turbulent time scale.

Return to isotropy of the orientation vectors is similar but operates on a vector rather than a tensor term:

$$A_i = -\frac{1}{\tau_R}\left(\frac{C_Q}{1+C_B\nu/\nu_T}\right)\left[3\frac{\overline{q_iq_k}}{\overline{q^2}}-\delta_{ki}\right]q_k \tag{9}$$

The tensor $\overline{q_iq_k}/\overline{q^2}$ represents the average orientations of the eddies. When one of the diagonal components of this tensor is large, then most of the eddies point in that direction, or the eddies that point in that direction have small sizes (and hence large q^2). The value of C_Q is typically larger than C_R and is set to 2.75 in this work. Isotropy in the OEC model therefore occurs when the oriented stresses become isotropic, but also when the eddy orientations become uniformly distributed on a sphere. Note that mean flow gradients tend to distort the orientation distribution, and random mixing by turbulence tends to return orientations to the isotropic state.

In order to maintain orthogonality (or fluctuating incompressibility), a term must be added to the stress equation to account for the orientation return to isotropy:

$$\left(R_{lj}\frac{q_i}{q^2}+R_{li}\frac{q_j}{q^2}\right)(A_l) \tag{10}$$

Appendix B shows how this term makes $\frac{\partial(R_{ij}q_j)}{\partial t}=0$, which implies that orthogonality is preserved by the transport equations if the system starts in an orthogonal state which is necessary in order to be a consistent incompressible initial condition.

For flows far from features such as solid boundaries or shear free interfaces, accounting for viscous diffusion is straightforward. The Laplacian of the effective

viscosity $\nu+\nu_T$ and the quantity of interest—the eddy orientation vector or Reynolds stress tensor—will suffice:

$$+\left[(\nu+\nu_T)\,R_{ij,k}\right]_{,k} \text{ and } +\frac{1}{3}\left[(\nu+\nu_T)\,q_{i,k}\right]_{,k} \tag{11}$$

The factor of 1/3 is included to be consistent with the dissipation models but has no real theoretical basis for inclusion in the diffusion term. It is also important for the OEC model to respond properly to system rotation either due to the mean flow or due to a non-inertial frame. This may be achieved by modifying the decay rate of the orientation vectors to account for system rotation:

$$-\frac{1}{\tau_R}\left[\frac{\overline{\left(q_k\Omega_k^*\right)^2/q^2}}{20\overline{q^2}\,\overline{K}+0.25\left(\Omega_k^*\right)^2}\right]q_i \tag{12}$$

where the absolute vorticity is $\Omega_k^*=\varepsilon_{ijk}\overline{u}_{k,j}+\Omega_i$. The term $q_k\Omega_k^*$ implies that turbulence that is two-dimensional (*i.e.* has one component of the orientation always zero) will not be affected by system rotation perpendicular to that plane (as theory dictates). At low rotation rates this term becomes negligible, with the value of 'low' dictated by the constant 20. At high rotation rates the term in square parenthesis approaches 4/3, leading to a theoretical decay rate for the kinetic energy of 6/13. A value of 0.4 (rather than 0.25) for the second constant leads to a kinetic energy decay rate of 3/5 (as cited in [18]) The two numerical constants in the Eq. 12 were determined empirically through the work of Perot and Chartrand [19].

The complete transport equations for the Oriented-Eddy Collision model can now be constructed. The orientations obey the equation

$$\begin{aligned} q_{i,t}+\left(\overline{u}_j q_i\right)_{,j} &= -q_k\overline{u}_{k,i}-\frac{1}{3}\left(\alpha\nu\overline{q^2}+\frac{1}{\tau_R}\left\{1+\frac{3\overline{\left(q_k\Omega_k^*\right)^2/q^2}}{20.0\overline{q^2}\,\overline{K}+0.25\left(\Omega_k^*\right)^2}\right\}\right)q_i \\ &\quad +\frac{1}{3}\left[(\nu+\nu_T)\,q_{i,k}\right]_{,k}-\frac{1}{\tau_R}\left(\frac{C_Q}{1+C_B\nu/\nu_T}\right)\left[3\frac{\overline{q_iq_k}}{\overline{q^2}}-\delta_{ki}\right]q_k \end{aligned} \tag{13}$$

Similarly, the evolution equation for the Reynolds stress tensor becomes

$$\begin{aligned} R_{ij,t}+\left(\overline{u}_k R_{ij}\right)_{,k} &= \left[\overline{u}_{i,k}+\left(\frac{q_iq_l}{q^2}-\delta_{il}\right)2\overline{u}_{l,k}^*\right]R_{kj}+\left[\overline{u}_{j,k}+\left(\frac{q_jq_l}{q^2}-\delta_{jl}\right)2\overline{u}_{l,k}^*\right]R_{ki} \\ &\quad -\left(\alpha\nu\overline{q^2}+\frac{1}{\tau_R}\right)R_{ij}-\frac{1}{\tau_R}\left(\frac{C_R}{1+C_B\nu/\nu_T}\right)\left[R_{ij}-\overline{K}\left(\delta_{ij}-\frac{q_iq_j}{q^2}\right)\right] \\ &\quad +\left(R_{lj}\frac{q_i}{q^2}+R_{li}\frac{q_j}{q^2}\right)A_l+\left[(\nu+\nu_T)\,R_{ij,k}\right]_{,k} \end{aligned} \tag{14}$$

This paper does not consider solid boundaries and boundary conditions. That topic will be addressed in a later paper.

2.3 Initial conditions

The initial conditions for the eddy orientation vectors and stresses must be addressed. In theory, the more orientations used in the model, the better the representation of the underlying physics. Based on the number of eddies N, each cell in the computational domain is populated with N Reynolds stress tensors, and N eddy vectors. For isotropic initial conditions, the eddy orientations are sampled uniformly on a sphere. The magnitude of the eddy vectors governs the dissipation, so these vectors must initially be scaled to have the correct magnitude for a given initial kinetic energy and Reynolds number. The initial eddy vectors are scaled by the positive root to the following quadratic equation (with roots β):

$$\left[\nu\left(\overline{q^2K^0}\right)\alpha\right]\beta^2+\left[\left(\overline{K^0}\right)^{\frac{3}{2}}\overline{q^2}^{\frac{1}{2}}\right]\beta=\frac{\left(\overline{K^0}\right)^2}{\nu Re_T^0} \tag{15}$$

where $\overline{K^0}$ and Re_T^0 are the average initial kinetic energy and turbulent Reynolds number. Recall that the average eddy magnitude is calculated by $\overline{q^2}=\frac{1}{N}\sum q^2$.

The Reynolds stresses are set by the initial average Reynolds stress tensor $\overline{R_{ij}^0}$ and the corresponding eddy orientation is set by the equation,

$$R_{ij}^{IC}=3\left[\overline{R_{ij}^0}-\frac{q_kq_i}{q^2}\overline{R_{jk}^0}-\frac{q_kq_j}{q^2}\overline{R_{ik}^0}+\frac{q_s\overline{R_{st}^0}q_t}{q^2}\delta_{ij}\right]-\frac{3}{2}\left(\delta_{ij}-\frac{q_iq_j}{q^2}\right)\overline{R_{kk}^0} \tag{16}$$

These initial stresses are always orthogonal to the corresponding orientation. They have the correct kinetic energy for each orientation in as much as they sum to the initial Reynolds stress ($\overline{R_{ij}^0}$) when the orientations are distributed on a sphere (that is, when they are isotropic).

3 Model Validation

3.1 Regular and rotating isotropic decay

The most basic test of the OEC model is isotropic decaying turbulence. Direct numerical simulation data from de Bruyn Kops and Riley [20] is employed. The initial kinetic energy for this case is $\overline{K}^0=0.075\ \mathrm{m^2/s^2}$ and the initial turbulent Reynolds number is $Re_T^0=665$. The OEC model accurately predicts the decay of the turbulent kinetic energy, even though the decay process is non-linear and therefore an entirely modeled phenomenon (Fig. 1). In addition, nine cases of turbulent rotating decay with varying turbulent Rossby and Reynolds numbers, from Wigeland and Nagib [21], are calculated. The initial conditions are summarized in Table 1, noting the definition of the turbulent Reynolds number $Re_T\equiv\overline{K}^2/\nu\overline{\varepsilon}$ and turbulent Rossby number $Ro_T\equiv\overline{\varepsilon}/\left(|\Omega_i|\,\overline{K}\right)$.

The OEC model predicts the decay of turbulent kinetic energy for all nine cases within reasonable accuracy compared to data from Wigeland and Nagib. Figures 2, 3 and 4 show the model's performance. A more marked deviation from the benchmark

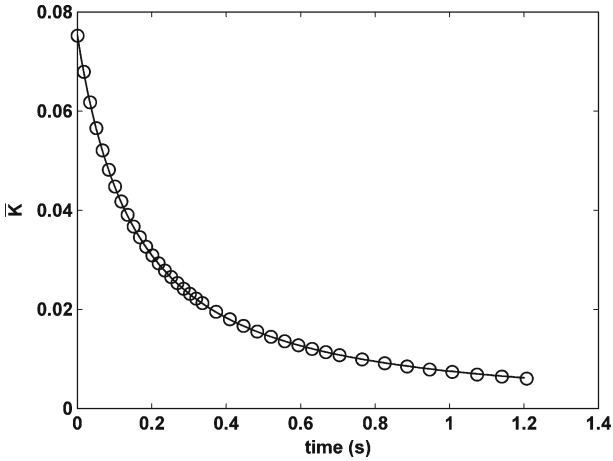

Fig. 1 Isotropic, homogeneous decay of kinetic energy predicted by the OEC model (—) compared to DNS data from de Bruyn Kops and Riley [20] (○)

data are noted for the three cases with the highest rotation rate, especially at long times.

Rotating decay was also tested with data taken from Jacquin et al. [22]. Note that only the highest Reynolds number case is shown here, as agreement at lower Reynolds numbers was excellent and tested previously. For the case considered, the initial dissipation was $\overline{\varepsilon} = 30.96\ \mathrm{m}^2/\mathrm{s}^3$, the initial kinetic energy $\overline{K} = 0.444\ \mathrm{m}^2/\mathrm{s}^2$, and the initial kinematic viscosity $\nu = 1.51\mathrm{E}\text{-}5\ \mathrm{m}^2/\mathrm{s}$. The case began with a turbulent Reynolds number of $\mathrm{Re}_T = 457$ and initial turbulent Rossby number of $\mathrm{Ro}_T = 1.10$. Figure 5 compares the OEC model's predictions to data from Jacquin et al. (case C), the highest Reynolds number considered. Even at high Reynolds number the model deviates from the experimental data by less than 5%.

The results of Mansour, Cambon, and Speziale's [23] simulations of turbulent rotating decay were employed as a final test of the OEC model's ability to predict such flows. The initial conditions for the four cases considered are listed in Table 2. Thoroughly testing the model's ability to accurately predict rotating decay was necessary as the rotating dissipation model must remain stable for long times in order to compute cases such as steady state shear flow.

Figure 6 shows the OEC model's prediciton of normalized kinetic energy as a function of time when subjected to the conditions presented in Table 2. Interestingly, cases A and C, which were run at the highest turbulent Rossby numbers, show the closest agreement to Mansour, Cambon, and Speziale's data and matched to within 5%. Cases B and D, with lower Rossby numbers, showed agreement only

Table 1 Initial conditions for Wigeland and Nagib [21]

	A			B			C		
$\overline{\varepsilon}\ (\mathrm{m}^2/\mathrm{s}^3)$	14.85	14.67	14.94	2.96	3.49	3.36	2.77	3.36	22.26
$\overline{K}\ (\mathrm{m}^2/\mathrm{s}^2)$	0.098	0.0975	0.105	0.045	0.0462	0.051	0.029	0.033	0.096
$\nu\ (\mathrm{m}^2/\mathrm{s})$	1.85E-5	1.8E-5	1.85E-5	1.85E-5	1.85E-5	1.85E-5	1.85E-5	1.85E-5	1.85E-5
Re_T	36	36	41	38	34	43	17	18	23
Ro_T	∞	7.52	1.78	∞	3.77	0.82	∞	5.09	2.9
$\lvert\Omega_i\rvert$	0	20	80	0	20	80	0	20	80

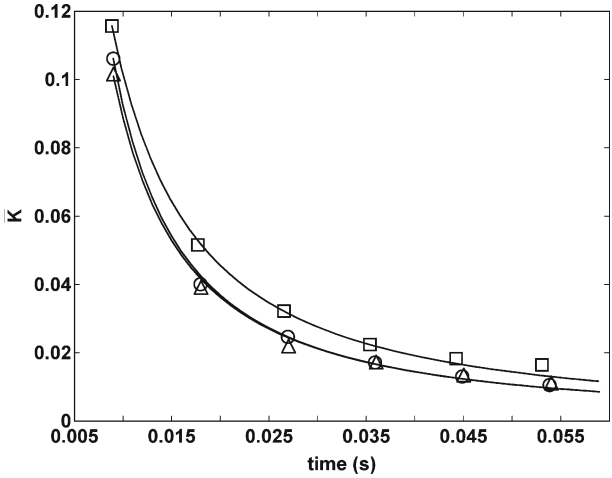

Fig. 2 Rotating and non-rotating decay of kinetic energy from Wigeland and Nagib [21], case A: $|\Omega_i| = 0$ (○), $|\Omega_i| = 20$ (Δ), $|\Omega_i| = 80$ (□), compared to predictions from the OEC model (—)

to within 10%. Note that data from Mansour et al. [23] cases C and D run for relatively brief periods of time, possibly indicating difficulty in attaining accurate DNS simulations, especially case C (□) which only provides data up to 0.8 s.

3.2 Rapid distortion theory

The addition of orientation information to the OEC model enables it to accurately capture turbulence in highly non-equilibrium conditions, such as those described by rapid distortion theory (RDT). Amongst the RDT cases considered and used for validation were the following: Axisymmetric expansion, akin to an expansion in a wind tunnel in directions transverse to the mean flow; axisymmetric contraction in which the turbulent flow is contracted in the transverse directions, plane strain, and finally shear. The four cases are summarized in Table 3 and shown Figs. 7, 8, 9 and 10.

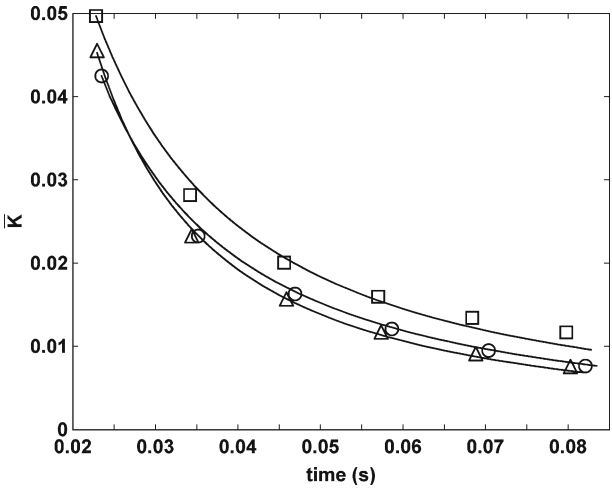

Fig. 3 Rotating and non-rotating decay of kinetic energy from Wigeland and Nagib [21], case B $|\Omega_i| = 0$ (○), $|\Omega_i| = 20$ (Δ), $|\Omega_i| = 80$ (□), compared to predictions from the OEC model (—)

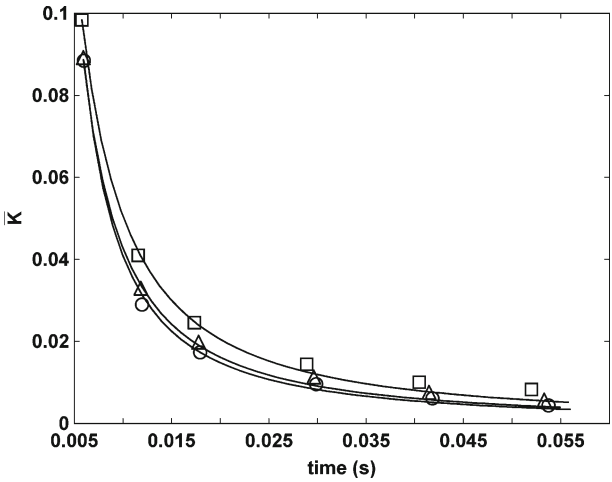

Fig. 4 Rotating and non-rotating decay of kinetic energy from Wigeland and Nagib [21], case C: $|\Omega_i| = 0$ (○), $|\Omega_i| = 20$ (Δ), $|\Omega_i| = 80$ (□), compared to predictions from the OEC model (—)

The tensor $\overline{u}_{i,j}$ is the mean velocity gradient tensor applied to the turbulent flow to produce rapid distortion, and S a scalar quantity that controls the amount of strain. The exact RDT solutions can be found in numerous references.

One final case related to axisymmetric expansion, investigated by Lee and Reynolds [24] among others, is that of *slow* axisymmetric expansion. Challenges inherent to modeling such a flow are detailed by Kassinos et al. [25]. Single point closure methods have difficulty capturing slow strain as the Reynolds stress anisotropy is greater than that found in rapidly distorted cases. The OEC model was subjected to slow axisymmetric expansion with $SK^0/\varepsilon^0 = 0.41$ and compared to RDT case at a much higher $SK^0/\varepsilon^0 = 20.0$, both at a turbulent Reynolds number of $Re_T^0 = 200$. Similar to the observations made by Kassinos and Reynolds [3, 26], slow axisymmetric strain exhibits higher initial anisotropy when compared to standard RDT. Figure 11 shows this interesting phenomenon, described in detail by Kassinos et al. [25].

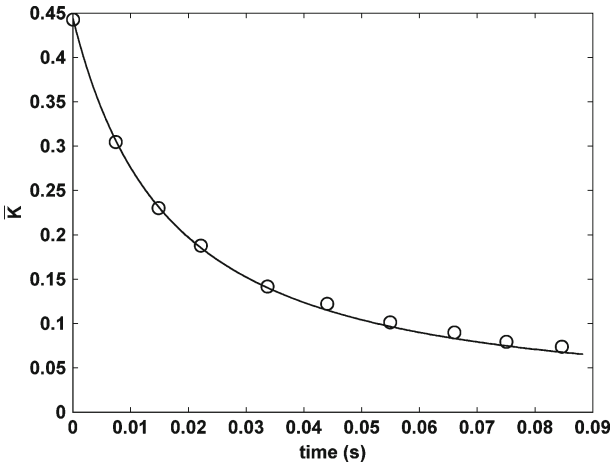

Fig. 5 Rotating and non-rotating decay of kinetic energy from Jacquin et al. [22] (○) with $Ro_T = 1.10$ (case C) compared to predictions from the OEC model (—)

Table 2 Initial conditions for Mansour et al. [23] rotating decay cases

	A	B	C	D
$\overline{\varepsilon}\,(\mathrm{m}^2/\mathrm{s}^3)$	0.93		0.95	
$\overline{K}\,(\mathrm{m}^2/\mathrm{s}^2)$	0.964		0.977	
$\nu\,(\mathrm{m}^2/\mathrm{s})$	3.67E-2		1.49E-2	
Re_T	27.2		67.1	
Ro_T	0.37	0.037	0.24	0.1

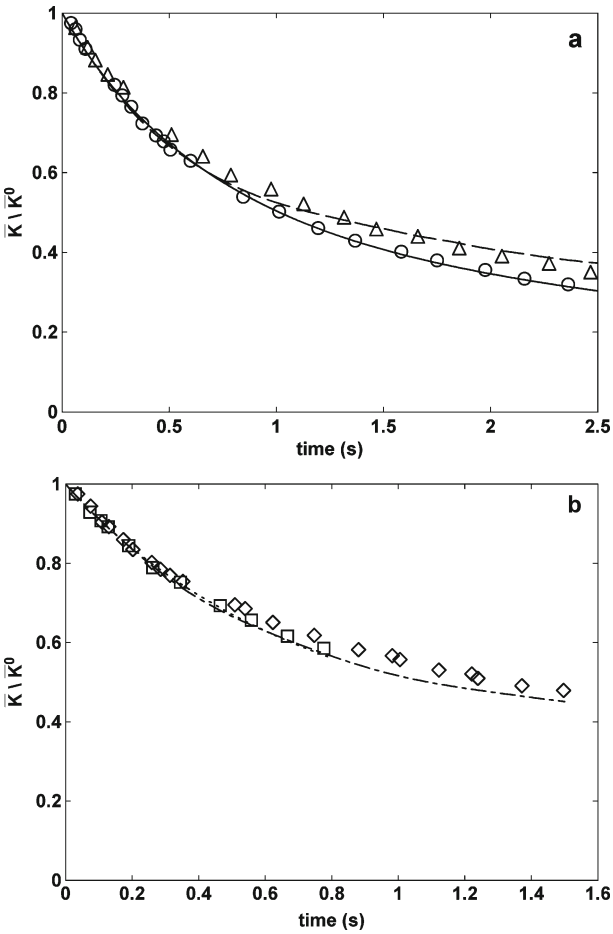

Fig. 6 The OEC model's predictions for normalized kinetic energy of rotating decay compared to data from Mansour et al. [23]. **a** Cases A (○) and B (Δ) data from Mansour et al. compared to OEC's predictions for cases A (—) and B (- - -). **b** Mansour cases C (□) and D (◇), compared to OEC's predictions, (- - -) and (· · ·) respectively

Table 3 Rapid distortion theory cases used for testing the OEC model

	Axisymmetric contraction	Axisymmetric expansion	Plane strain
$\overline{u}_{i,j}$	$\begin{bmatrix} S & 0 & 0 \\ 0 & -\frac{1}{2}S & 0 \\ 0 & 0 & -\frac{1}{2}S \end{bmatrix}$	$\begin{bmatrix} -2S & 0 & 0 \\ 0 & S & 0 \\ 0 & 0 & S \end{bmatrix}$	$\begin{bmatrix} S & 0 & 0 \\ 0 & -S & 0 \\ 0 & 0 & 0 \end{bmatrix}$

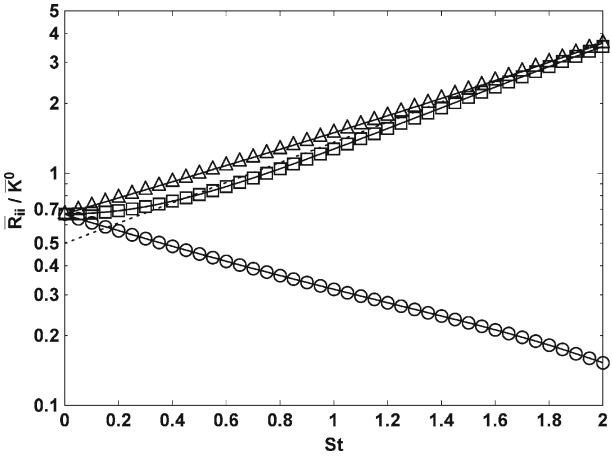

Fig. 7 Plane strain data of principal Reynolds stresses. Symbols from RDT: $\overline{R}_{11}/\overline{K}^0$ (○), $\overline{R}_{22}/\overline{K}^0$ (Δ), $\overline{R}_{33}/\overline{K}^0$ (□), compared to the OEC model (—), and the theoretical limit $^1/_2 e^{St}(\cdots)$

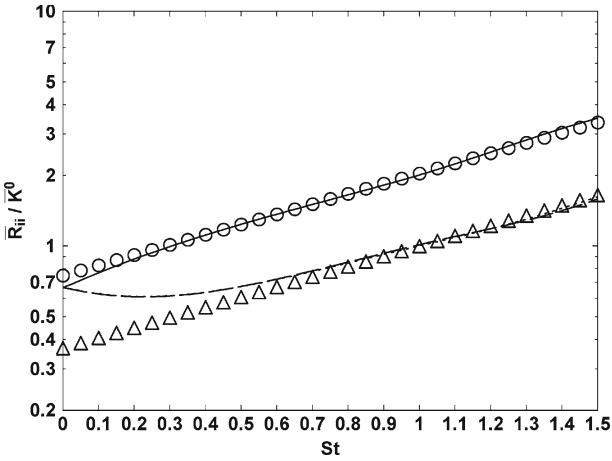

Fig. 8 Axisymmetric expansion data of principal Reynolds stresses as predicted by the OEC model: $\overline{R}_{11}/\overline{K}^0$ (–), $\overline{R}_{22}/\overline{K}^0 = \overline{R}_{33}/\overline{K}^0$ (- - -), compared to the theoretical long-time asymptotic growth rates : $e^{[St+\log(0.75)]}$ (○), $e^{[St+\log(0.36)]}$ (Δ)

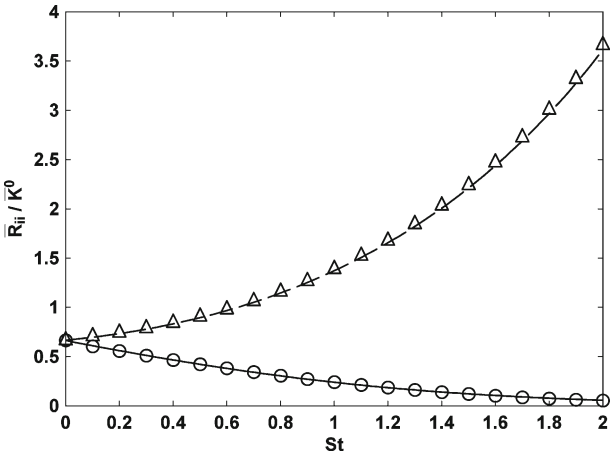

Fig. 9 Axisymmetric contraction data of principal Reynolds stresses: RDT results, $\overline{R}_{11}/\overline{K}^0$ (○), $\overline{R}_{22}/\overline{K}^0 = \overline{R}_{33}/\overline{K}^0$ (Δ), compared to predictions from the OEC model $\overline{R}_{11}/\overline{K}^0$ (—) and $\overline{R}_{22}/\overline{K}^0 = \overline{R}_{33}/\overline{K}^0$ (- - -)

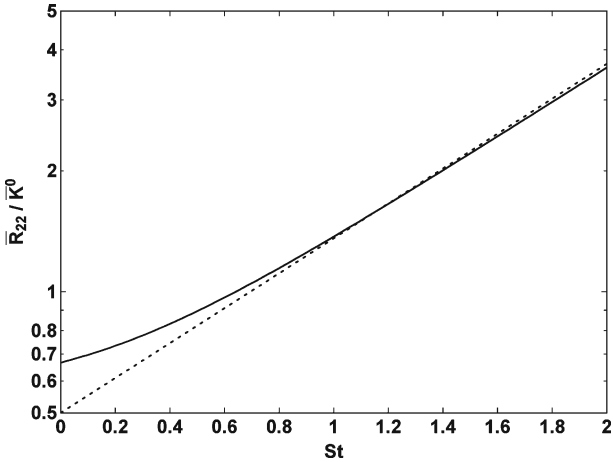

Fig. 10 A closer look at the OEC model's prediction of $\overline{R}_{22}/\overline{K}^0$ (—) compared to the asymptotic growth rate $\frac{1}{2}e^{St}$ $(\cdots)$ for axisymmetric contraction

3.3 Return to isotropy

Data from Le Penven et al. [27] is widely used to test return-to-isotropy. The flow, which is initially isotropic, is rapidly strained to an anisotropic state and then allowed to relax back toward isotropy. The velocity gradient tensor employed for the two cases considered is shown in Table 4 and causes very different types of anisotropy. Case A has one large stress value and case B has two large stress values. The initial values for the Reynolds number are not provided in the data, and were deduced by what produced the correct conditions at the end of the straining region.

Agreement between data from L. Le Penven, J. N. Gence, and G. Comte-Bellot, case A [27] and the OEC model is within 8%, as shown in Fig. 12. While case B (Fig. 13) shows less agreement, the model's prediction for the return to isotropy of stress tensor is reasonably accurate for both cases, and possibly within the error levels of the experiment and initial condition specification.

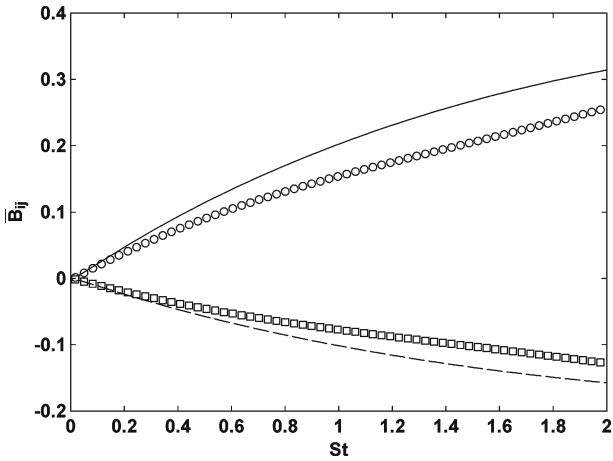

Fig. 11 Anisotropy predictions of the OEC model for slow axisymmetric expansion, $SK^0/\varepsilon^0 = 0.41$: $\overline{B}_{11}$(—), $\overline{B}_{22} = \overline{B}_{33}$ (- - -) and $\overline{B}_{33}$ $(\cdots)$. Compared to RDT with $SK^0/\varepsilon^0 = 20.0$: $\overline{B}_{11}$ (○), $\overline{B}_{22} = \overline{B}_{33}$ (□). Anisotropy is defined as $\overline{B}_{ij} = \overline{R}_{ij}/2\overline{K} - \frac{1}{3}\delta_{ij}$

Table 4 Summary of initial conditions for shear flow cases Le Penven et al. [27]

	Le Peven et al. case A	Le Peven et al. case B
$S\overline{K}/\overline{\varepsilon}$	0.43	0.33
Re_T	612	846
$\overline{u}_{i,j}$	$\begin{bmatrix} 5.48 & 0 & 0 \\ 0 & 1.99 & 0 \\ 0 & 0 & -7.47 \end{bmatrix}$	$\begin{bmatrix} 8.86 & 0 & 0 \\ 0 & -2.36 & 0 \\ 0 & 0 & 6.50 \end{bmatrix}$

3.4 Shear

The shear flow benchmark comes from the 64×256×64 (X×Y×Z) simulation data of Matsumoto et al. [28], the initial conditions and strain tensor of which are detailed in Table 5. Unlike the previous return cases, the flow is subject to a constant shear that persists for all time. The first case is at a very low turbulent Reynolds number, $\mathrm{Re}_T = 18$, and is only considered for a short dimensionless time, $St \leq 4$. The data are

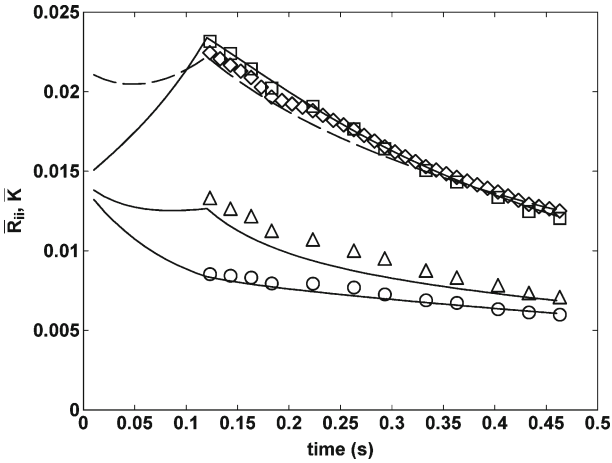

Fig. 12 Principal Reynolds stress and kinetic energy decay. Symbols are data from L. Le Penven, J. N. Gence, and G. Comte-Bellot, case A [27]: $\overline{R}_{11}$ (○), $\overline{R}_{22}$ (Δ), $\overline{R}_{33}$ (□), $\overline{K}$ (◇); compared to the OEC model: $\overline{R}_{ii}$ (—), $\overline{K}$ (- - -)

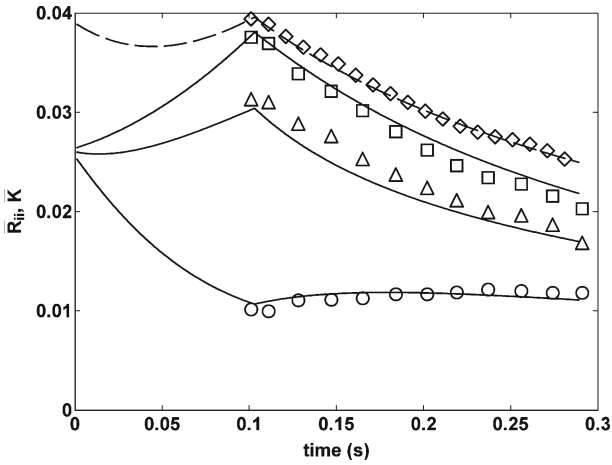

Fig. 13 Principal Reynolds stress and kinetic energy decay. Symbols are data from L. Le Penven, J. N. Gence, and G. Comte-Bellot, case B [27]: $\overline{R}_{11}$ (○), $\overline{R}_{22}$ (Δ), $\overline{R}_{33}$ (□), $\overline{K}$ (◇); compared to predictions from the OEC model: $\overline{R}_{ii}$ (—), $\overline{K}$ (- - -)

Table 5 Initial conditions for the shear flow cases of Matsumoto et al. [28]

$S\overline{K}/\overline{\varepsilon}$	30.6	4.71
Re_T	18.18	152
$\overline{u}_{i,j}$	$\begin{bmatrix} 0 & 28.28 & 0 \\ 0 & 0 & 0 \\ 0 & 0 & 0 \end{bmatrix}$	$\begin{bmatrix} 0 & 30.0 & 0 \\ 0 & 0 & 0 \\ 0 & 0 & 0 \end{bmatrix}$

presented in the form of the anisotropy tensor, $\overline{A}_{ij} = \left(\overline{R}_{ij}/\overline{K}\right) - 2\delta_{ij}/3$. Of primary interest is the OEC model's ability to predict the shear stress, $\overline{A}_{12}$, over short times (Fig. 14).

Agreement between OEC's prediction of the evolution of stresses and available data from Matsumoto et al. is reasonable and within 4%. The ability of the model to remain accurate over such a short time is not surprising since this is almost an RDT case. The higher Reynolds number case, $\mathrm{Re}_T = 152$, runs for a much longer time and is the more difficult case. The data are also presented in the form of the anisotropy

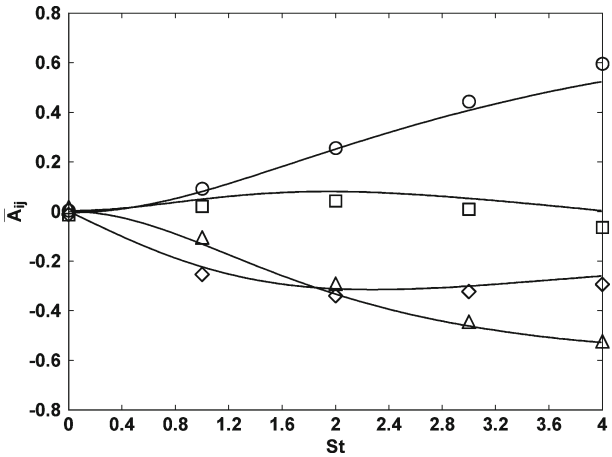

Fig. 14 Anisotropy data $\overline{A}_{ij} = \left(\overline{R}_{ij}/\overline{K}\right) - 2\delta_{ij}/3$ at $\mathrm{Re}_T = 18$ from Matsumoto et al. [28]. $\overline{A}_{11}$ (○), $\overline{A}_{22}$ (Δ), $\overline{A}_{33}$ (□), $\overline{A}_{12}$ (◇); compared to results from the OEC model (—)

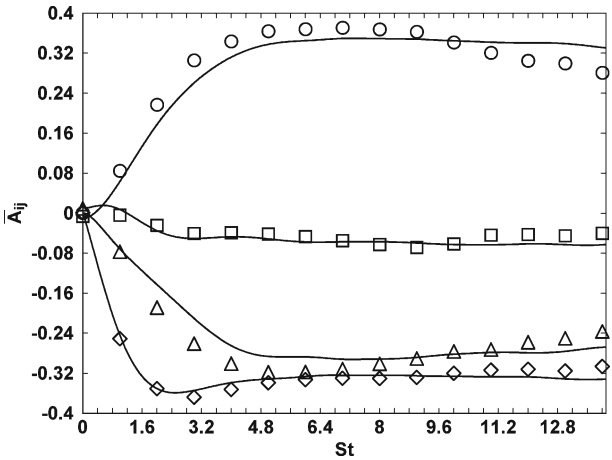

Fig. 15 Anisotropy data $\overline{A}_{ij} = \left(\overline{R}_{ij}/\overline{K}\right) - 2\delta_{ij}/3$ at $Re_T = 152$from Matsumoto et al. [28]. $\overline{A}_{11}$ (○), $\overline{A}_{22}$ (Δ), $\overline{A}_{33}$ (□), $\overline{A}_{12}$ (◇); compared to results from the OEC model (—)

tensor and shown in Fig. 15 against predictions of the OEC model. Unlike the low Reynolds number case, the current data extends to relatively long dimensionless time $St \approx 14.4$. By time $St \approx 8$ the flow has reached a steady, anisotropic state and should remain so indefinitely. Agreement between the OEC model and data from Matsumoto et al. is quite good considering the challenging nature of the benchmark. It is interesting to note that $\overline{A}_{11}$ (○) and $\overline{A}_{22}$ (Δ) from Matsumoto et al. appear to begin to return despite the presence of shear. This behavior may be due to the finite size of the simulation domain for the DNS data.

4 Discussion

This paper demonstrates the OEC model's ability to capture both equilibrium and non-equilibrium turbulent flows. In addition, the model remains stable at long times and when subjected to highly anisotropic flow conditions. The OEC model precisely captures isotropic, homogeneous decaying turbulence as well as the rotating decay cases. Further refinement of the dissipation-like term which handles frame rotation may result in predictions even closer to experimental/DNS data. The model is capable of returning the theoretical solution to turbulent flows in the rapid distortion theory limit, setting it apart from most other turbulence models. The inclusion of turbulent structure information is imperative to capturing linear turbulence, and this physical information is captured in the OEC model by using turbulent eddy orientation information. While adding to the overall cost and complexity of the method, the benefits are obvious. Casting the OEC model in a form similar to familiar Reynolds stress transport models aids comprehension and enables the user to employ traditional solution methods when implementing the model.

It should be noted that the OEC model is an order of magnitude more computationally demanding than existing RANS models. This implies that in a turbulent Navier-Stokes calculation, the computational effort required to calculate the turbulence with the OEC model is now roughly equal to the computational effort required to calculate the mean flow. In our estimation, this is not particularly expensive, and corresponds to the appropriate level of effort since the turbulence physics represents roughly half of the total physics of most turbulent flow problems. The OEC modeling approach is still orders of magnitude less computationally demanding than large eddy simulation (LES). The OEC modeling approach therefore occupies a useful niche in the cost versus accuracy tradeoff, allowing much higher levels of predictive accuracy than traditional RANS models at a cost significantly less than LES. Unlike typical Reynolds stress models, the large number of equations means that each equation is not particularly stiff.

Acknowledgements The authors would like to thank the Office of Naval Research for their direct support of this work under grant number N00014-08-1-0275. The National Science Foundation also contributed to the support of this research effort.

Appendix A: Basis for the OEC Model

We begin with the simplified transport equation for the two-point correlation $Q_{ij}(x,r) \equiv \overline{u_i'(x)u_j'(\tilde{x})}$ (Eq. 3 in the text),

$$\frac{\partial Q_{ij}}{\partial t} = -\left(\bar{u}_{i,k} + 2\varepsilon_{kil}\Omega_l\right) Q_{kj} - \left(\bar{u}_{j,k} + 2\varepsilon_{kjl}\Omega_l\right) Q_{ik} - r_l \frac{\partial \bar{u}_k}{\partial x_l}\frac{\partial Q_{ij}}{\partial r_k} + \left(\frac{\partial \overline{u_j'p}(\tilde{x},-r)}{\partial r_i} - \frac{\partial \overline{u_i'p}}{\partial r_j}\right) + 2\nu\frac{\partial^2 Q_{ij}}{\partial r_k \partial r_k} + \left(\frac{\partial Q_{(ik)j}}{\partial r_k} - \frac{\partial Q_{i(kj)}}{\partial r_k}\right) \tag{17}$$

and recall that incompressibility requires

$$\frac{\partial Q_{ij}}{\partial r_j} = 0 \tag{18}$$

The pressure velocity correlation equation can be expressed as

$$\frac{\partial \overline{u_i'p}}{\partial r_j \partial r_j} = -2\bar{u}^*_{k,j}(\tilde{x})\frac{\partial Q_{ij}}{\partial r_k} - \frac{\partial^2}{\partial r_k \partial r_k}\left(\overline{u_i'(x)u_k'(\tilde{x})u_j'(\tilde{x})}\right) + \overline{u_i'(x)f_{j,j}(\tilde{x})}. \tag{19}$$

The two point fluctuating velocity correlation Q_{ij}, as well as the pressure correlation $\overline{u_i'p}$, and the triple correlation $\overline{u_i'(x)u_k'(\tilde{x})u_j'(\tilde{x})}$, may be decomposed as

$$Q_{ij} = \sum_0^\infty R_{ij}\frac{\partial F}{\partial(\mathbf{q}\cdot\mathbf{r})},\ \overline{u_i'p} = \sum_0^\infty u_i'pF,\ \text{and}$$

$$\overline{u_i'(x)u_k'(\tilde{x})u_j'(\tilde{x})} = \sum_0^\infty u_i'u_k'u_j'F \tag{20}$$

respectively. Note the difference between Eqs. 19 and 5 in the text, where here $\eta = (\mathbf{q}\cdot\mathbf{r})$ and $F = F(\eta) = F(\mathbf{q}\cdot\mathbf{r})$ is some positive function. We note several useful derivatives involving the decompositions above,

$$\frac{\partial Q_{ij}}{\partial r_k} = \sum \frac{\partial^2 F}{\partial(q_k r_k)^2} q_k R_{ij}, \quad \frac{\partial \overline{u_i'p}}{\partial r_j} = \sum \frac{\partial F}{\partial(q_j r_j)} q_j u_i' p,$$

$$\frac{\partial^2 \overline{u_i'p}}{\partial r_j \partial r_j} = \sum \frac{\partial^2 F}{\partial(q_j r_j)^2}(q_j)^2 u_i' p \tag{21}$$

noting that the summation limits have been dropped and $\eta = (\mathbf{q}\cdot\mathbf{r}) = (q_i r_i)$. Starting with Eq. 19 and using the decompositions in (A4) and derivatives in Eq. 21 and simplifying the second derivative of the triple correlation, we arrive at

$$\sum \frac{\partial^2 F}{\partial(q_j r_j)^2} q^2 u_i' p = -2\bar{u}^*_{k,j}(\tilde{x}) \sum \frac{\partial^2 F}{\partial(q_k r_k)^2} q_k R_{ij} - \sum u_i' u_k' u_j' q_k q_j \frac{\partial^2 F}{\partial(r_k q_k)^2} \tag{22}$$

noting the last term in Eq. 19 has been neglected. Dividing though by $\sum[(\partial^2 F/\partial(q_j r_j)^2)(q_j)^2]$ yields

$$\overline{u_i' p} = -2\bar{u}^*_{k,j}(\tilde{x})\frac{q_k}{q^2}R_{ij} - \frac{q_k q_j}{q^2}u_i' u_k' u_j' \tag{23}$$

Moving on to the two point velocity correlation equation, substituting decompositions and evaluating derivatives yields

$$\begin{aligned}
&\sum\left(R_{ij,t}\frac{\partial F}{\partial(\mathbf{q}\cdot\mathbf{r})} + \frac{\partial^2 F}{\partial(\mathbf{q}\cdot\mathbf{r})^2}q_{l,t}r_l R_{ij}\right)\\
&\quad = \left(2\varepsilon_{ikl}\Omega_l - \bar{u}_{i,k}\right)\sum\left(R_{kj}\frac{\partial F}{\partial(\mathbf{q}\cdot\mathbf{r})}\right) + \left(2\varepsilon_{jkl}\Omega_l - \bar{u}_{j,k}\right)\sum\left(R_{ik}\frac{\partial F}{\partial(\mathbf{q}\cdot\mathbf{r})}\right)\\
&\qquad -r_l\bar{u}_{k,l}\sum\frac{\partial^2 F}{\partial(q_k r_k)^2}q_k R_{ij} - \sum u_j' u_k' u_i' q_k\frac{\partial F}{\partial(\mathbf{q}\cdot\mathbf{r})} - \sum u_i' u_k' u_j' q_k\frac{\partial F}{\partial(\mathbf{q}\cdot\mathbf{r})}\\
&\qquad -\sum q_i u_j' p\frac{\partial F}{\partial(\mathbf{q}\cdot\mathbf{r})} - \sum q_j u_i' p\frac{\partial F}{\partial(\mathbf{q}\cdot\mathbf{r})} + 2\nu\sum R_{ij}q^2\frac{\partial^3 F}{\partial(\mathbf{q}\cdot\mathbf{r})^3}
\end{aligned} \tag{24}$$

noting again that in Eq. 24 the forcing terms have been neglected. Equation 24 must be simplified. This can be achieved by moving all terms to the right hand side of the equation, grouping with respect to $\sum \partial F/\partial\left(\mathbf{q}\cdot\mathbf{r}\right)$ (and higher order derivatives), and recalling $\overline{u}^*_{i,j} = \overline{u}_{i,j} + \varepsilon_{ikj}\Omega_k$,

$$\begin{aligned}
0 = \sum\frac{\partial F}{\partial(\mathbf{q}\cdot\mathbf{r})}\Bigg[&-R_{ij,t} + \left[\bar{u}_{i,k} + 2\bar{u}^*_{l,k}\left(\frac{q_i q_l}{q^2} - \delta_{il}\right)\right]R_{jk} + \left[\bar{u}_{j,k} + 2\bar{u}^*_{l,k}\left(\frac{q_j q_l}{q^2} - \delta_{jl}\right)\right]R_{ik}\\
&-u_i' u_k' u_l'\left(\delta_{jl} - \frac{q_j q_l}{q^2}\right)q_k - u_j' u_k' u_l'\left(\delta_{il} - \frac{q_i q_l}{q^2}\right)q_k\Bigg]\\
-\sum\frac{\partial^2 F}{\partial(\mathbf{q}\cdot\mathbf{r})^2}r_l\left[q_{l,t} + \bar{u}_{k,l}q_k\right]R_{ij} &+ \sum\frac{\partial^3 F}{\partial(\mathbf{q}\cdot\mathbf{r})^3}2\nu k^2 R_{ij}
\end{aligned} \tag{25}$$

In order to arrive at the fundamental basis for the OEC model, we must assume the flow is subjected to rapid distortion. This is sensible considering the basis for the model returns the RDT equations. To begin with, terms involving the triple correlation are removed along with the viscous term involving $\partial^3 F/\partial\left(\mathbf{q}\cdot\mathbf{r}\right)^3$. This reduces Eq. 25 to

$$\begin{aligned}
0 = \sum\frac{\partial F}{\partial(\mathbf{q}\cdot\mathbf{r})}&\Bigg[\overbrace{-R_{ij,t} + \left[\bar{u}_{i,k} + 2\bar{u}^*_{l,k}\left(\frac{q_i q_l}{q^2} - \delta_{il}\right)\right]R_{jk} + \left[\bar{u}_{j,k} + 2\bar{u}^*_{l,k}\left(\frac{q_j q_l}{q^2} - \delta_{jl}\right)\right]R_{ik}}^{\text{Expression "Y"}}\Bigg]\\
-\sum\frac{\partial^2 F}{\partial(\mathbf{q}\cdot\mathbf{r})^2}r_l&\overbrace{\left[q_{l,t} + \bar{u}_{k,l}q_k\right]}^{\text{Expression "Z"}}R_{ij}
\end{aligned} \tag{26}$$

In Eq. 26, two expressions have been labeled, "Y" and "Z". Equation 26 represents an infinite number of equations involving $\mathbf{q}$ and $\mathbf{r}$. As such, a collection of equations can be assembled representing this summation,

$$\begin{aligned}
0 &= \frac{\partial F}{\partial(\mathbf{q}\cdot\mathbf{r})}(q_1, r_1)\, Y_1(q_1) + \frac{\partial F}{\partial(\mathbf{q}\cdot\mathbf{r})}(q_2, r_1)\, Y_2(q_2) + \ldots \\
&\quad + \frac{\partial^2 F}{\partial(\mathbf{q}\cdot\mathbf{r})^2}(q_1, r_1)\, Z_1(q_1) + \frac{\partial^2 F}{\partial(\mathbf{q}\cdot\mathbf{r})^2}(q_2, r_1)\, Z_2(q_2) + \ldots \\
0 &= \frac{\partial F}{\partial(\mathbf{q}\cdot\mathbf{r})}(q_1, r_2)\, Y_1(q_1) + \frac{\partial F}{\partial(\mathbf{q}\cdot\mathbf{r})}(q_2, r_2)\, Y_2(q_2) + \ldots \\
&\quad + \frac{\partial^2 F}{\partial(\mathbf{q}\cdot\mathbf{r})^2}(q_1, r_2)\, Z_1(q_1) + \frac{\partial^2 F}{\partial(\mathbf{q}\cdot\mathbf{r})^2}(q_2, r_2)\, Z_2(q_2) + \ldots \\
0 &= \frac{\partial F}{\partial(\mathbf{q}\cdot\mathbf{r})}(q_1, r_3)\, Y_1(q_1) + \frac{\partial F}{\partial(\mathbf{q}\cdot\mathbf{r})}(q_2, r_3)\, Y_2(q_2) + \ldots \\
&\quad + \frac{\partial^2 F}{\partial(\mathbf{q}\cdot\mathbf{r})^2}(q_1, r_3)\, Z_1(q_1) + \frac{\partial^2 F}{\partial(\mathbf{q}\cdot\mathbf{r})^2}(q_2, r_3)\, Z_2(q_2) + \ldots
\end{aligned} \tag{27}$$

Equation set 27 can be assembled in to a linear system:

$$\begin{bmatrix}
\frac{\partial F}{\partial(\mathbf{q}\cdot\mathbf{r})}(q_1, r_1) + \frac{\partial F}{\partial(\mathbf{q}\cdot\mathbf{r})}(q_2, r_1) + \ldots + \frac{\partial^2 F}{\partial(\mathbf{q}\cdot\mathbf{r})^2}(q_1, r_1) + \frac{\partial^2 F}{\partial(\mathbf{q}\cdot\mathbf{r})^2}(q_2, r_1) + \ldots \\
\frac{\partial F}{\partial(\mathbf{q}\cdot\mathbf{r})}(q_1, r_2) + \frac{\partial F}{\partial(\mathbf{q}\cdot\mathbf{r})}(q_2, r_2) + \ldots + \frac{\partial^2 F}{\partial(\mathbf{q}\cdot\mathbf{r})^2}(q_1, r_2) + \frac{\partial^2 F}{\partial(\mathbf{q}\cdot\mathbf{r})^2}(q_2, r_2) + \ldots \\
\frac{\partial F}{\partial(\mathbf{q}\cdot\mathbf{r})}(q_1, r_3) + \frac{\partial F}{\partial(\mathbf{q}\cdot\mathbf{r})}(q_2, r_3) + \ldots + \frac{\partial^2 F}{\partial(\mathbf{q}\cdot\mathbf{r})^2}(q_1, r_3) + \frac{\partial^2 F}{\partial(\mathbf{q}\cdot\mathbf{r})^2}(q_2, r_3) + \ldots \\
\vdots
\end{bmatrix}
\times \begin{bmatrix} Y_1(q_1) \\ Y_2(q_2) \\ \vdots \\ Z_1(q_1) \\ Z_2(q_2) \\ \vdots \end{bmatrix} = \begin{bmatrix} 0 \\ 0 \\ \vdots \\ 0 \\ 0 \\ \vdots \end{bmatrix} \tag{28}$$

Considering the restrictions placed upon the function $F(\mathbf{q}\cdot\mathbf{r})$, $Y_1(q_1)$, $Y_2(q_2)$,... and $Z_1(q_1)$, $Z_2(q_2)$,... must all equate to zero in order to satisfy Eq. 28. This implies that for *any* $\mathbf{q}$ and $\mathbf{r}$

$$\begin{aligned}
Y_i(q_i) &= -R_{ij,t} + \left[\overline{u}_{i,k} + 2\overline{u}^*_{l,k}\left(\frac{q_i q_l}{q^2} - \delta_{il}\right)\right] R_{jk} \\
&\quad + \left[\overline{u}_{j,k} + 2\overline{u}^*_{l,k}\left(\frac{q_j q_l}{q^2} - \delta_{jl}\right)\right] R_{ik} = 0 \\
Z_i(q_i) &= q_{l,t} + \overline{u}_{k,l} q_k = 0
\end{aligned} \tag{29}$$

Thus, equation set 29 returns the desired RDT equations and forms the fundamental basis for the OEC model. Note that neglecting the viscous term in Eq. 25 is not strictly necessary and the argument above still holds if the term is included in Eq. 26. This is because any Sturm-Liouville-type ordinary differential equation must obey $\partial^3 F/\partial\left(\mathbf{q}\cdot\mathbf{r}\right)^3 = \partial F/\partial\left(\mathbf{q}\cdot\mathbf{r}\right) + \left(\mathbf{q}\cdot\mathbf{r}\right)\left[\partial^2 F/\partial^2\left(\mathbf{q}\cdot\mathbf{r}\right)\right]$ and therefore $F\left(\mathbf{q}\cdot\mathbf{r}\right)$ must satisfy this condition.

The decomposition for the two-point velocity correlation $Q_{ij} = \sum R_{ij}\frac{\partial F}{\partial(\mathbf{q}\cdot\mathbf{r})}$ must also be considered in the continuity equation,

$$\frac{\partial}{\partial r_j}\left(\sum R_{ij}\frac{\partial F}{\partial(\mathbf{q}\cdot\mathbf{r})}\right) = 0 \tag{30}$$

Expanding the derivative and rearranging, we arrive at

$$\sum \frac{\partial^2 F}{\partial(\mathbf{q}\cdot\mathbf{r})^2} R_{ij} q_j = 0 \tag{31}$$

noting that that we are assuming homogeneous flow. By the same argument employed to arrive at Equation set 28, we conclude that $R_{ij}q_j = 0$ and therefore maintaining incompressibility in a homogeneous flow is akin to ensuring orthogonality between R_{ij} and q_j.

Appendix B: Ensuring Orthogonality with the OEC Transport Equations

Equation 31 requires that the transport equations for R_{ij} and q_j maintain orthogonality between the two quantities for all time. More succinctly, it is necessary that

$$\frac{\partial}{\partial t}\left(R_{ij}q_j\right) = 0 \tag{32}$$

In order to ensure Eq. 32 is satisfied, Expression (10) was added to the Reynolds stress transport equation (Eq. 14 above). Expanding Eq. 32 illustrates this,

$$\begin{aligned}
\frac{\partial}{\partial t}\left(R_{ij}q_j\right) &= q_j\frac{\partial R_{ij}}{\partial t} + R_{ij}\frac{\partial q_j}{\partial t} \\
&= q_j\Bigg\{-\left(\overline{u}_k R_{ij}\right)_{,k} + \left[\overline{u}_{i,k} + \left(\frac{q_i q_l}{q^2} - \delta_{il}\right)2\overline{u}^*_{l,k}\right]R_{kj} \\
&\quad + \left[\overline{u}_{j,k} + \left(\frac{q_j q_l}{q^2} - \delta_{jl}\right)2\overline{u}^*_{l,k}\right]R_{ki} - \left(\alpha\nu\overline{q^2} + \frac{1}{\tau_R}\right)R_{ij} \\
&\quad - \frac{C_R}{\tau_R}\left(\frac{1}{1 + C_B\nu/\nu_T}\right)\left[R_{ij} - \overline{K}\left(\delta_{ij} - \frac{q_i q_j}{q^2}\right)\right] \\
&\quad + \left(R_{lj}\frac{q_i}{q^2} + R_{li}\frac{q_j}{q^2}\right)A_l + \left[\left(\nu + \nu_T\right)R_{ij,k}\right]_{,k}\Bigg\}
\end{aligned}$$

$$
\begin{aligned}
&+R_{ij}\Bigg\{-\left(\overline{u}_k q_j\right)_{,k}-q_l\overline{u}_{l,j}\\
&\quad-\frac{1}{3}\alpha\nu\overline{q^2}+\frac{1}{\tau_R}1+\frac{3\overline{\left(q_l\Omega_l^*\right)^2/q^2}}{20.0\overline{q^2}\,\overline{K}+0.25\left(\Omega_l^*\right)^2}q_j\\
&\quad+\frac{1}{3}\left[\left(\nu+\nu_T\right)q_{j,l}\right]_{,l}-\frac{C_Q}{\tau_R}\left(\frac{1}{1+C_B\nu/\nu_T}\right)\left[3N_{lj}-\delta_{lj}\right]q_l\Bigg\}
\end{aligned}
\tag{33}
$$

Equation 33 is cumbersome and must be simplified. To begin with, we again assume homogeneous turbulence and therefore neglect the viscous terms as well as any expression involving the gradient of the mean velocity. Multiplying through by q_j and R_{ij}, Eq. 33 reduces to

$$
\begin{aligned}
q_j\frac{\partial R_{ij}}{\partial t}+R_{ij}\frac{\partial q_j}{\partial t}&=q_j\left[\overline{u}_{i,k}+\left(\frac{q_iq_l}{q^2}-\delta_{il}\right)2\overline{u}_{l,k}^*\right]R_{kj}+q_j\left[\overline{u}_{j,k}+\left(\frac{q_jq_l}{q^2}-\delta_{jl}\right)2\overline{u}_{l,k}^*\right]R_{ki}\\
&\quad-q_j\left(\alpha\nu\overline{q^2}+\frac{1}{\tau_R}\right)R_{ij}-q_j\frac{C_R}{\tau_R}\left(\frac{1}{1+C_B\nu/\nu_T}\right)\\
&\quad\times\left[R_{ij}-\overline{K}\left(\delta_{ij}-\frac{q_iq_j}{q^2}\right)\right]+q_j\left(R_{lj}\frac{q_i}{q^2}+R_{li}\frac{q_j}{q^2}\right)A_l-R_{ij}q_l\overline{u}_{l,j}\\
&\quad-\frac{1}{3}R_{ij}\alpha\nu\overline{q^2}+\frac{1}{\tau_R}1+\frac{3\overline{\left(q_l\Omega_l^*\right)^2/q^2}}{20.0\overline{q^2}\,\overline{K}+0.25\left(\Omega_l^*\right)^2}q_j\\
&\quad-R_{ij}\frac{C_Q}{\tau_R}\left(\frac{1}{1+C_B\nu/\nu_T}\right)\left[3N_{lj}-\delta_{lj}\right]q_l
\end{aligned}
\tag{34}
$$

If we assume that the stress tensor and eddy orientation vector begin orthogonal $R_{ij}q_j\big|_{t=0}=0$ (which the code ensures), then all terms in Eq. 34 which involve this product must be zero initially. This further simplifies Eq. 34,

$$
\begin{aligned}
q_j\frac{\partial R_{ij}}{\partial t}+R_{ij}\frac{\partial q_j}{\partial t}&=q_j\overline{u}_{j,k}R_{ki}+R_{li}A_l-R_{ij}q_l\overline{u}_{l,j}\\
&\quad-R_{ij}\frac{C_Q}{\tau_R}\left(\frac{1}{1+C_B\nu/\nu_T}\right)\left[3N_{lj}-\delta_{lj}\right]q_l
\end{aligned}
\tag{35}
$$

By substituting the definition of the eddy orientation vector return-to-isotropy A_l (Eq. 9) into Eq. 35,

$$
\begin{aligned}
q_j\frac{\partial R_{ij}}{\partial t}+R_{ij}\frac{\partial q_j}{\partial t}&=q_j\overline{u}_{j,k}R_{ki}+R_{li}\left[\frac{C_Q}{\tau_R}\left(\frac{\nu_T}{\nu_T+C_B\nu}\right)\left[3N_{kl}-\delta_{kl}\right]q_k\right]\\
&\quad-R_{ij}q_l\overline{u}_{l,j}-R_{ij}\frac{C_Q}{\tau_R}\left(\frac{1}{1+C_B\nu/\nu_T}\right)\left[3N_{lj}-\delta_{lj}\right]q_l
\end{aligned}
\tag{36}
$$

and rearranging subscripts it is easily shown that $q_j \frac{\partial R_{ij}}{\partial t} + R_{ij} \frac{\partial q_j}{\partial t} = \frac{\partial}{\partial t}\left(R_{ij} q_j\right) = 0$ and thus the transport equations maintain orthogonality between q_j and R_{ij} for homogeneous turbulent flows.

References

1. Reynolds, W.C.: Effects of rotation on homogeneous turbulence. In: Proceedings of the 10th Australian Fluids Mechanics Conference, pp. KS 2.1–2.6. Melbourne (1989)
2. Perot, J.B.: Turbulence modeling using body force potentials. Phys. Fluids **11**(9), 2645–2656 (1999)
3. Kassinos, S.C., Reynolds, W.C.: One-point modeling of rapidly deformed homogeneous turbulence. Proc. R. Soc. London A **451**, 87–104 (1995)
4. Reynolds, W.C., Kassinos, S.C.: A particle representation model for the deformation of homogeneous turbulence. Center for Turbulence Research, Stanford University/NASA Ames Research Center (1996)
5. Akylas, E., Kassinos, S.C.: Advances in particle representaiton modeling of homogeneous turbulence. From linear PRM version to the interacting viscoelastic IPRM. In: ERCOFTAC: New Approaches in Modeling Multiphase Flows and Dispersion Turbulence, Fractal Methods, and Synthetic Turbulence, vol. 18 (2011)
6. Pope, S.B. Van Sloten, P.R.: PDF modeling for inhomogeneous turbulence with exact representation of rapid distortions. Phys. Fluids **9**(4), 1085–1105 (1996)
7. Jasak, H.: Error analysis and estimation for the finite volume method with applications to fluid flows. Imperial College of Science, Technology and Medicine, London, England, Ph.D. Thesis (1996)
8. Rusche, H.: Computational fluid dynamics of dispersed two-phase flows at high phase fractions. Ph.D. thesis, Imperial College of Science, Technology and Medicine, London, England (2002)
9. Lumley, J.L., Tennekes, H.: A First Course in Turbulence. Cambridge, Massachusetts (1972)
10. Pope, S.B.: Turbulent Flows. Cambridge University Press, New York (2000)
11. Deissler, R.G.: Problem of steady state shear flow turbulence. Phys. Fluids **8**(3), 391–398 (1965)
12. de Bruyn Kops, S.M., Perot, J.B.: Modeling turbulent dissipation at low and moderate Reynolds numbers. J. Turbul. **7**(69), 1–14 (2006)
13. Saffman, P.G.: On the spectrum and decay of random two-dimensional vorticity distributions at large Reynolds number. Stud. Appl. Math. **50**, 377–383 (1971)
14. Saffman, P.G.: The large-scale structure of homogeneous turbulence. J. Fluid Mech. **27**(3), 581–593 (1967)
15. Perot, J.B.: Determination of the decay exponent in mechanically stirred isotropic turbulence. AIP Adv. **1**, 022104:1–18 (2011)
16. Chartrand, C., Perot, J.B.: Modeling return to isotropy using kinetic equations. Phys. Fluids **17**, 035101-1 (2005)
17. Rotta, J.: Statistische Theorie nichthomogener turbulenz. Z. Phys. A-Hadron Nucl. **129**(6), 547–572 (1951)
18. Mininni, P.D., Teitelbaum, T.: The decay of turbulence in rotating flows. Phys. Fluids **23**, 065105:1–15 (2011)
19. Chartrand, C.C.: Eddy collision models for turbulence. Masters thesis, The University of Massachusetts, Amherst (2005)
20. Riley, J.J., de Bruyn Kops, S.M.: Direct numerical simulation of laboratory experiments in isotropic turbulence. Phys. Fluids **10**, 2125–2127 (1998)
21. Nagib, H.M., Wigeland, R.A.: Effects of rotation on decay of turbulence. Bull. Am. Phys. Soc. **23**, 998 (1978)
22. Leuchter, O., Cambon, C., Mathieu, J., Jacquin, L.: Homogeneous turbulence in the presence of rotation. J. Fluid Mech. **220**, 1–52 (1990)
23. Cambon, C., Speziale, C.G., Mansour, N.N.: Theoretical and computational study of rotating isotropic turbulence. In: Sarkar, S., Speziale, C.G., Gatski, T.B. (eds.) Studies in Turbulence. Springer-Verlag (1992)
24. Reynolds, W.C., Lee, M.J.: Numerical experiments on the structure of homogeneous turbulence. Thermosciences, Deparment of Mechanical Engineering, Stanford University, TF-24 (1985)

25. Reynolds, W.C., Rogers, M.M., Kassinos, S.C.: One-point turbulence structure tensors. J. Fluid Mech. **428**, 213–248 (2001)
26. Reynolds, W.C., Kassinos, S.C.: A Structure-Based Model with Stropholysis Effects. Center for Turbulence Research Annual Research Briefs (1998)
27. Gence, J.N., Comte-Bellot, G. Le Penven, L.: On the approach to isotropy of homogeneous turbulence: effect of the partition of kinetic energy among the velocity components. In: Davis, S.H., Lumley, J.L. (eds.) Frontiers in Fluid Mechanics, p. 1. Springer (1984)
28. Nagano, Y., Tsuji, T., Matsumoto, A.: Direct numerical simulation of homogeneous turbulent shear flow. In: 5th Symposium on Computational Fluid Dynamics, pp. 361–364 (1991)